OPEN ACCESS
IOP Publishing | International Atomic Energy Agency
Nuclear Fusion
Nucl. Fusion **60** (2020) 106021 (11pp)
https://doi.org/10.1088/1741-4326/aba72b

ECCD-induced sawtooth crashes at W7-X

M. Zanini[1], H.P. Laqua[1], H. Thomsen[1], T. Stange[1], C. Brandt[1], H. Braune[1], K.J. Brunner[1], G. Fuchert[1], M. Hirsch[1], J. Knauer[1], U. Höfel[1], S. Marsen[1], E. Pasch[1], K. Rahbarnia[1], J. Schilling[1], Y. Turkin[1], R.C. Wolf[1,2], A. Zocco[1] and W7-X team[1,a]

[1] Max-Planck-Institut für Plasmaphysik, 17491 Greifswald, Germany
[2] Zentrum für Astronomie und Astrophysik,Technische Universität Berlin, 10623 Berlin, Germany

E-mail: marco.zanini@ipp.mpg.de

Received 30 March 2020, revised 11 June 2020
Accepted for publication 17 July 2020
Published 9 September 2020

Abstract

The optimised superconducting stellarator W7-X generates its rotational transform by means of external coils, therefore no toroidal current is necessary for plasma confinement. Electron cyclotron current drive experiments were conducted for strikeline control and safe divertor operation. During current drive experiments periodic and repetitive crashes of the central electron temperature, similar to sawtooth crashes in tokamaks, were detected. Measurements from soft x-ray tomography and electron cyclotron emission show that the crashes are preceded by weak oscillating precursors and a displacement of the plasma core, consistent with a $(m, n) = (1, 1)$ mode. The displacement occurs within 100 μs, followed by expulsion and redistribution of the core into the external part of the plasma. Two types of crashes, with different frequencies and amplitudes are detected in the experimental program. For these non-stationary parameters a strong dependence on the toroidal current is found. A 1-D heuristic model for current diffusion is proposed as a first step to explain the characteristic crash time. Initial results show that the modelled current diffusion timescale is consistent with the initial crash frequency and that the toroidal current rise shifts the position where the instability is triggered, resulting in larger crash amplitudes.

Keywords: stellarator, sawtooth, ECCD

(Some figures may appear in colour only in the online journal)

1. Introduction

The superconducting optimised stellarator Wendelstein 7-X (W7-X) [1, 2] is mainly heated by a flexible electron cyclotron resonance heating (ECRH) system, composed of 10 gyrotrons, able to deliver up to 7.5 MW of power into the plasma [3]. The region where the energy transfer from the microwaves to the electrons occurs is well localised and can be changed by steering the launcher mirrors, thus making ECRH a versatile tool. When the injection is oblique to the magnetic axis in the toroidal direction, a selective heating of electrons is possible and a net toroidal current (electron cyclotron current drive, ECCD) is generated [4, 5]. In principle, a toroidal current is not needed for plasma confinement in stellarators, since the rotational transform is generated by means of external coils. However, since the W7-X divertor concept relies on the existence of magnetic island chains at the plasma edge, which occur at resonant values of the rotational transform, ECCD is one of the principal tools for strike lines control [6–9], by compensating or counter-acting the intrinsic plasma currents [10]. ECCD experiments have been conducted at W7-X in OP1.1 and

[a] See Klinger et al 2019 (https://doi.org/10.1088/1741-4326/ab03a7) for the W7-X team.

OP1.2 campaigns. In such experiments, repetitive crashes of the central electron temperature were observed: these crashes have similar characteristics as sawtooth oscillations observed in tokamaks [11] and, under certain conditions, in current carrying stellarators [12–14]. While small sawteeth can be beneficial, countering or avoiding impurity accumulation [15, 16], large amplitude crashes can be detrimental for plasma performances. The sawtooth instability is generally associated with an unstable $(m, n) = (1, 1)$ mode [17], where m and n are respectively the poloidal and toroidal mode numbers. The first explanation of this phenomenon was proposed by Kadomtsev [18]. The core is displaced by the formation and growth of an $m = n = 1$ magnetic island around it. The temperature drop is caused by the expulsion of the hot core, resulting in a flattening of the pressure profile inside the new plasma core, which in turn reduces the central current density removing the instability drive again. This model, however, turned out to be unable to explain certain experimental observations, such as characteristic timescales, measured post-crash rotational transform profiles ($\iota = \iota/2\pi = 1/q$, where q is the safety factor) or the existence of $(1, 1)$ postcursors, hence other models have been proposed [19].

In W7-X, operational magnetic configurations have been designed to avoid major resonances in the rotational transform profile. During ECCD experiments, the driven current itself can locally modify ι, thus making the plasma susceptible to MHD instabilities.

Several experiments have been conducted in order to evaluate the impact of sawtooth oscillations on W7-X plasmas. In this work we present the analysis of a characteristic discharge, in order to elucidate the main features of sawtooth-like crashes in W7-X. These crashes are often preceded by a fast displacement of the plasma core, consistent with a $(m, n) = (1, 1)$ structure, but sometimes weak precursors can also be observed. The crash evolution is unchanged during the discharge, but the amplitude and the time interval between two events is found to be not constant in time. Comparing the amplitude and the location of the crashes, we identified two types of crashes: one affecting the central part of the plasma and another, stronger, extending the crashed volume to about 50 % of the effective radius.

Possible mechanisms for W7-X sawteeth have been recently proposed, whether purely current-density-gradient-driven [20, 21] or current and pressure driven [22]. In both cases, non-ideal corrections to Ohm's law (collisional or kinetic) and $\iota \approx 1$ are the key excite instabilities with low mode numbers.

The paper is structured as follows: in section 2, a description of W7-X and the main diagnostics is provided. In section section 3 we present a typical ECCD experimental program, where sawtooth-like crashes were detected. In section section 4 we discuss the relation between crash parameters as a function of time and the main differences between the two observed types of crashes. Finally, in section section 5 we discuss the effects of current drive on the rotational transform profile and the relation between the current and the crash parameters.

2. Experimental setup

The magnetic field of W7-X is generated by 50 superconducting non-planar coils and 20 planar coils. The current in each coil type can be indipendently set, thus allowing a wide range of magnetic field configurations. The minor radius varies from 0.49 m to 0.55 m and the major radius is 5.5 m, resulting in an aspect ratio of the W7-X stellarator of around 10. The magnetic field on the axis in the bean-shaped plane is generally around 2.5 T. The rotational transform depends on the choosen magnetic configuration, but for the analysed discharge, the so-called *standard configuration* was used, which has a rotational transform value of 0.85 in the core and 0.97 at the last closed flux surface (LCFS).

W7-X is a low shear stellarator which relies on the natural island chain at the edge. Therefore the control of the total toroidal current is necessary in order to prevent component damages due to a misalignment of the strikelines on the divertor plates. Plasma heating is mainly provided by ECRH. Up to 10 microwave beams are injected with a frequency of 140 GHz. The gyrotrons are able to selectively operate in O-mode or in X-mode. ECRH launchers are installed in two modules in the proximity of the so-called bean-shaped planes, where the magnetic field has the maximum strength. The flexibility of the ECRH system allows to deposit the power at different poloidal locations of the plasma cross-section. It is also possible to inject microwave beams in toroidal direction to create (ECCD). The current drive efficiency decreases as the electron collisionality increases, therefore the experiment presented here was conducted at low density (about $2 \cdot 10^{19}\,\mathrm{m}^{-3}$). The electron temperature was about 5 keV in the core for $1.2 - 1.8$ MW of injected power. Due to low coupling between electrons and ions, the ion temperature was about 1 keV. Co-ECCD was applied to the plasmas presented here, i.e. the current was driven in a direction such that the rotational transform is increased.

This work mainly focuses on the experimental results obtained from electron cyclotron emission (ECE, with a sampling rate between 200 kHz and 1 MHz) [23] analysis, which is capable of radially resolving the fast and local changes of the electron temperature. A 1-D electron temperature (T_e) profile can be reconstructed by the measurement along the line of sight of the ECE diagnostic, viewing the plasma from the outboard side and crossing the plasma centre. The magnetic field increases with the distance to the receiver optics such that the ECE spectra can be ideally interpreted in terms of a local electron temperature, if the plasma behaves like a black body, i.e. the optical thickness is large. The ECE channels are mapped to the effective radius $r_{\mathrm{eff}} = \sqrt{\langle A \rangle / \pi}$ using the following definition: channels detecting at the outboard region of the plasma, namely the low field side (LFS), are labelled with

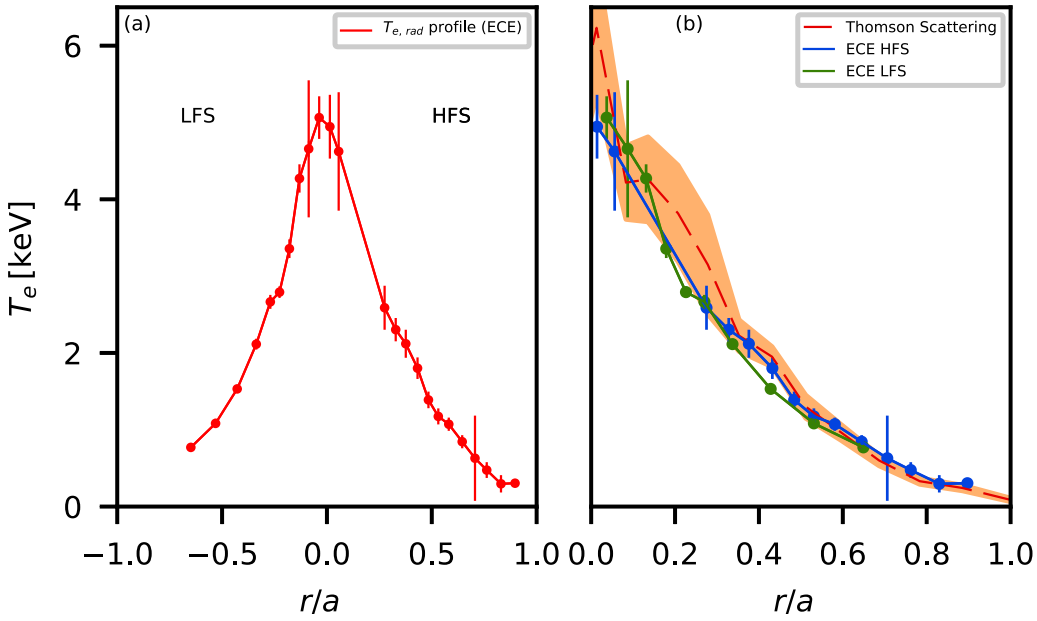

Figure 1. Left: Typical T_e profile, mapped to the radial position. Right: ECE profiles (blue for HFS and green for LFS) against a Thomson scattering profile (red).

negative radial position, while inboard (high field side, HFS) channels with a positive value. The mapping is performed taking into account diamagnetic effects, the Shafranov shift and the finite emission layer. These effects would introduce a significative shift from the HFS to the LFS if not taken into account. The T_e spectrum is estimated with a Bayesian modelling [24]. In figure 1(*a*) a typical T_e profile is plotted, while in figure 1(*b*) ECE data are compared to the Thomson scattering data. Both sides of the ECE profile agree with the Thomson scattering profile, especially at lower temperatures. At higher temperatures the HFS and LFS channels present some discrepancies which are however within the errorbars. The dominant uncertainty measurement is given by calibration errors, which are plotted in figure 1(*a*) along with the temperature profile itself. Calibration errors are much higher than the noise contribution, which is relatively small (less than 6 %) therefore only the absolute value of the measurement is affected. In this work ECE data are mainly used to study the relative signal drop due to a crash, therefore calibration errors do not affect the measurement quality.

The second main diagnostic is the x-ray tomography system. Plasma emission in the soft x-ray range ($1-12$ keV) is measured by an array of 20 pinhole cameras, each with 18 lines of sight, with a sample rate of 2 MHz. X-ray tomography is capable of reconstructing the evolution of the plasma emissivity in a poloidal plane [25].

Other major diagnostics used for this work are a single dispersion interferometer [26] which yields line integrated density measurement (sample rate of 100 kHz), continuous Rogowski coils for toroidal plasma current (sample rate of 50 kHz) and diamagnetic loops for the stored plasma energy (sample rate of 50 kHz) [27]. No direct measurements of the current density profile are available at the moment, therefore the ECCD profile is calculated using the ray-tracing code

Table 1. Main experimental program parameters for the discharge *20171206.025*.

Tor. Magnetic field (axis)	$B = -2.52$ T
EC Heating Power	$P = 1.2$ MW
Major radius	$R_0 = 5.5$ m
Minor radius	$a = 0.5$ m
Electron Temperature (axis)	$T_e = 5$ keV
Ion Temperature (axis)	$T_i = 1$ keV
Plasma energy	$W_{\mathrm{dia}} = 170$ kJ
Line int. density	$< n_e >= 2 \cdot 10^{19}\,\mathrm{m}^{-3}$
Toroidal current (max)	$I_{\mathrm{tor}} = -12$ kA
L/*R* time	$\tau \approx 5-10$ s
Resistive time	$\tau_\eta = 62$ s
Central β	$\beta_{\mathrm{max}} \approx 0.7\,\%$

TRAVIS [28]. It calculates ECRH propagation and absorbtion into the plasma, taking in account a pre-calculated magnetic equilibrium, for instance, using VMEC (Variational Moments Equilibrium Code [29]) and electron pressure profile. The current density profile evolution is then calculated resolving a diffusion equation, as discussed in section 5.

3. ECCD and sawtooth-like crashes at W7-X

Several current drive experiments have been conducted. A typical experiment is presented in detail in figure 2. The electron temperature in the core is around $5-6$ keV and line integrated density about $2-2.5 \cdot 10^{19}\,\mathrm{m}^{-3}$. At these T_e and n_e values, the coupling between ions and electrons is low, therefore the ion temperature is about 1 keV. In the experimental program *20171206.025* the plasma was initially heated by one ECRH beam in the centre (600 kW) and by two ECRH beams obliquely injected, leading to generate current

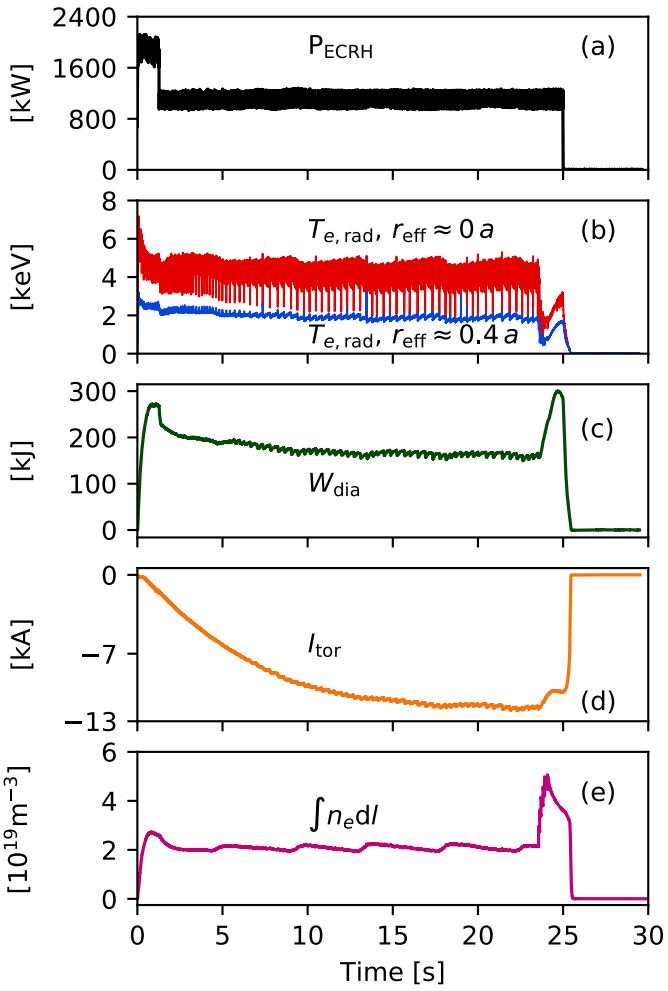

Figure 2. Overview plot of experimental program *20171206.025*. Sawtooth-like crashes are visible in the ECE channels, plotted in the second panel (core ECE channel in red and the ECE channel detecting at $r_{eff} \approx 0.3$ m in blue). Bigger crashes can be seen in the diamagnetic energy (third plot) and in the toroidal current (fourth plot). The line integrated density is plotted in the fifth plot, where density rise due to pellet injections is visible from $t = 23$ s.

drive. Because of the Doppler shift, the power deposition is slightly off-axis and calculations using TRAVIS show that the deposition is located at around 15 % of the effective radius, for approximately −14 kA of driven toroidal current. After some seconds the gyrotron providing the core ECRH beam dropped and the plasma was sustained until the end of the discharge by the two obliquely injected beams. Besides the heating power drop at 1.3 s and a phase with pellet injections from $t = 23$ s, density and plasma energy are relatively constant. The toroidal current is given by the sum of bootstrap current and the generated ECCD. Since the pressure gradient is relatively low, no strong contribution from the bootstrap current is expected (about $2-3$ kA, broadly distributed). The plasma behaves like an inductor which opposes changes of the magnetic flux, therefore the whole current does not develop suddenly, but evolves on the timescale of the *L*/*R* time ($\tau_{L/R}$), where $L = R_0\mu_0(\ln(8R_0/a) - 2)) \approx 18\,\mu$H and $R = 2\pi R_0(\int_0^a \sigma 2\pi r dr)^{-1} \approx 2\,\mu\Omega$ are the plasma inductance and resistance, with σ being the parallel Spitzer conductivity [30]. The toroidal current evolution can be described by the following equation:

$$I_{tor}(t) = I_{tor}(t \to \infty)(1 - e^{-t/\tau}). \quad (1)$$

$\tau_{L/R}$ is estimated to be between 5 s and 10 s. Finally, it can be noticed that the toroidal plasma current saturates around 15 s. In this phase, the main current component is created by ECCD and the experimental value is in good agreement with the one obtained by the ray-tracing code TRAVIS. Central temperature crashes started to appear after hundreds of milliseconds after the start of the plasma heating. While the dynamic of every crash shows the same features (i.e. strong T_e decrease in the centre, along with a slight increase on the external plasma region), the main crash parameters, such as frequency and amplitude change in time. An example, further discussed in section 4, can be seen in figure 3. In the selected time window (from 16 s to 17 s), it is possible to distinguish two main types of temperature crashes, according to their amplitude: in ECE timetraces, two big crashes can be distinguished between the minor crashes. The central temperature drops generally between 30–50 % and recovers in about 5–20 ms. Corresponding to the strong temperature crashes, a drop in the stored plasma energy (about 10 kJ, corresponding to 5 % of the whole energy) is detected by diamagnetic loops and the time for the energy to recover is on the order of 200 ms, one order of magnitude slower than the central temperature recovering time mentioned above.

The structure and the time evolution of the crashes are mainly studied using electron cyclotron emission, which allows high temporal (200 kHz for this experimental program) and spatial resolution. Soft x-ray tomographic reconstructions have been performed for the strongest events. Smaller events, such as the intermediate crashes in figure 3 are too weak and too localised to be detected by soft x-ray emission so far.

The crash is occasionally preceded by short living precursor oscillations ($2-6$ kHz) and in most of the cases by a displacement of the plasma core. Precursors have not been identified in x-ray data, while ECE data suggest the signal perturbation has an odd poloidal number. Timetraces of four ECE channels are plotted in figure 4. Two channels are high field side (HFS) channels and two are low field side (LFS) channels. It is possible to observe small amplitude precursors from $t = 2.7785$ s to $t = 2.7791$ s. The two core channels (channels 11 and 13) show T_e oscillations 180° out of phase, consistent with an odd poloidal number. An example of a crash without oscillating precursors is plotted in figure 5. In figure 5(*a*), the timetraces of the ECE channels show that no strong oscillating precursors are present before the crash. Instead, the plasma core undergoes a displacement, as plotted in red dashed line in figure 5(*b*) or depicted in the contour plot of figure 6, where the rapid movement of the core to the low field side is visible before the crash.

The core displacement evolves on a timescale of 100 μs. The analysis of different crashes shows that the core movement can happen in every poloidal direction. Having ECE only a 1-D horizontal line of sight, only horizontal movements of

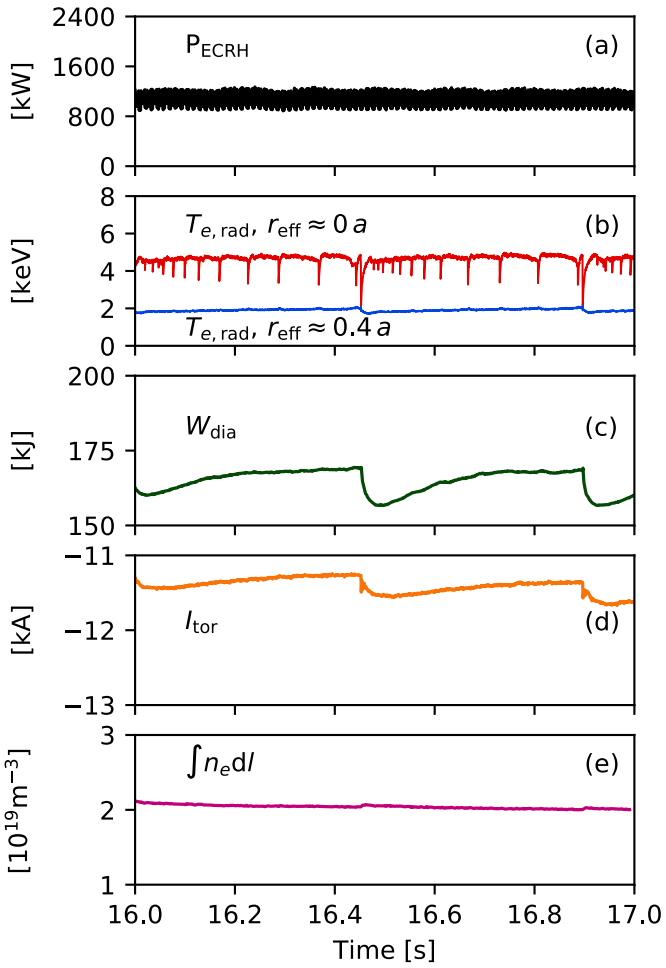

Figure 3. Zoom of the overview plot of figure 2, between 16 and 17s. Two types of crashes can be distinguished. The strong events at 16.4 and 16.9 s are also visible in the diamagnetic energy (third panel) and toroidal current (fourth panel).

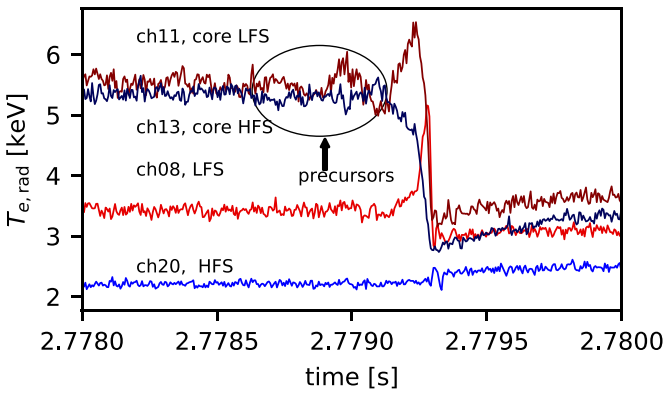

Figure 4. Precursor activity in *20171206.025* detected by ECE. The oscillation amplitude is small and generally relatively short. After the oscillating precursors, the core temperature displacement is visibile. Before the crashes, a strong increase of temperature is visible in the two low field side channels (ch08 in red and ch11 in dark red), while a decrease is detected in the high field side central channel (ch13, dark blue), indicating a fast movement of plasma centre from the core to the LFS.

the core can be detected, nonetheless soft x-ray tomography confirms the existence of vertical displacements. No relevant differences have been detected so far in these cases. The ECE radiometer and the x-ray camera array are placed almost 180 degrees apart in toroidal direction. We observed that an horizontal movement in the ECE from the core to the LFS (HFS) corresponds, in the x-ray tomography, to a movement from core to HFS (LFS). Comparing the movement directions of x-ray signals with respect to ECE signals (figures 6 and 7), we conclude that the toroidal mode number n has to be odd. Regarding the poloidal structure of the core movement, it creates a strongly asymmetric structure, typical for an $m = 1$ mode, as plotted in figure 5(b), time step II. The crash phase happens in 20 μs, in which core energy is redistributed outside the inversion radius (defined in figure 5(c)) and symmetry is restored (time step III in figure 5(a) and (b)). The T_e profile inside the crash region is almost flat and T_e is higher outside the inversion radius, with respect to the pre-crash profile. The re-heating phase (time step IV) depends on the amplitude of the crash and the involved region: for the crashes in this experimental program the typical time is about $5 - 20$ ms, faster than the time interval between two events. The soft x-ray tomographic reconstruction (4 μs of temporal resolution) displayed in figure 7 confirms the $m = 1$ structure detected by ECE and allows to better visualise the crash dynamics. The data presented here have been filtered by applying singular value decomposition (SVD) [31] to remove the dominant component of the emissity which, for this case, consisted of a constant value. After the displacemet phase, the tomograms show a poloidal propagation of the expelled core. The redistribution is not isotropic and occurs in the direction of the electron diamagnetic drift. Eventually, once the core expulsion has been completed, the SVD-filtered emissivity profile results in an hollow shape, followed by a recover of the electron temperature profile after the crash.

4. Crash pattern evolution

The characterisation of crash parameters, in particular amplitude and frequency, is crucial for future applications of ECCD in W7-X: the localisation and the amplitude of the crash are related to the released energy during this event. Therefore it is necessary to understand how these parameters change during the discharge. Looking at figure 2, apart from some minor changes in the density, the main changing parameter seems to be the toroidal current, which starts to saturate between 15 s and 20 s, reaching a value of −12 kA, consistent with TRAVIS calculations. We studied the evolution of the three main parameters: the crash frequency, the inversion radius and the maximum amplitude during a crash (figure 8). An example of how these parameters are defined can be seen in figure 5(c). The inversion radius is calculated for both HFS and LFS of the plasma and it is defined as the radial position where the temperature remains constant before and after the crash. The maximum amplitude, ΔT_e, is defined as the maximum relative change between the profile before and after the crash. Finally,

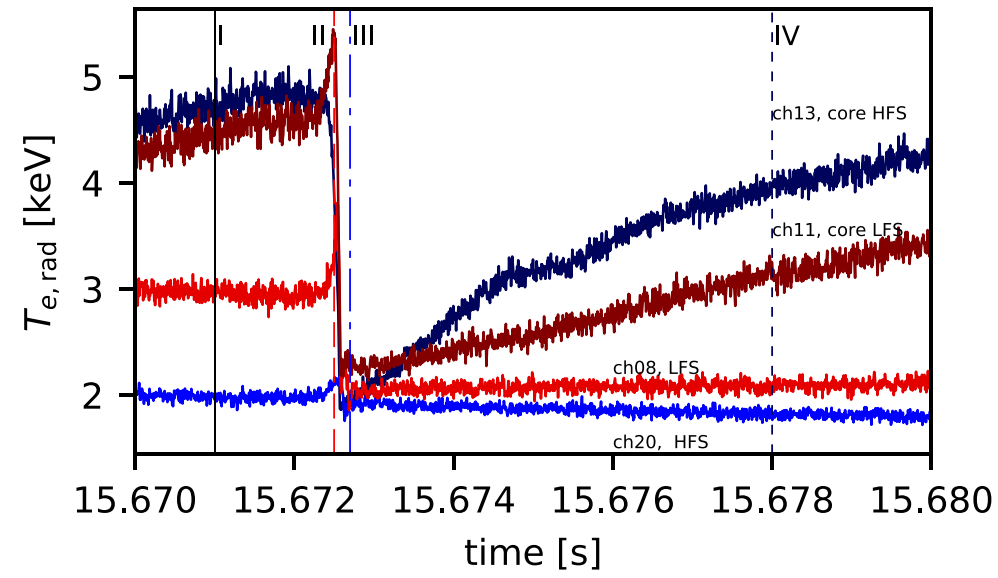

(a)

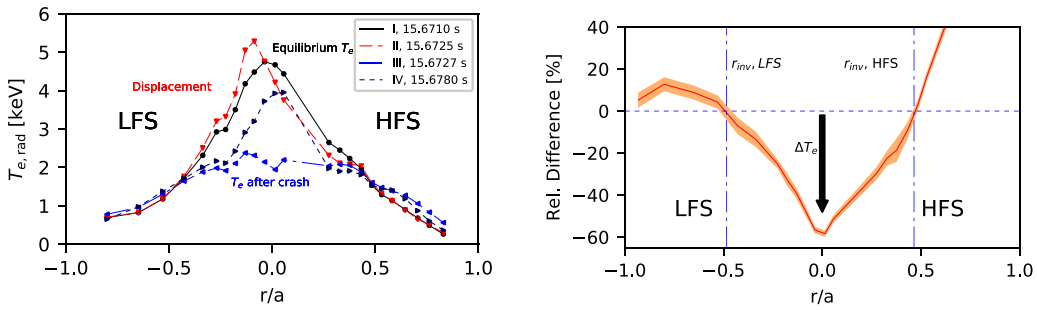

(b) (c)

Figure 5. (a): T_e evolution profile during a crash. Four ECE channels are plotted. Red-shaded timetraces correspond to LFS channels, while blue-shaded to HFS channels. Vertical lines represents the time points which have been used to reconstruct T_e profiles in (b). The timewindow for the profile average is 15 μs. I) represents the equilibrium profile, II) the profile during the displacement, III) the profile right after the crash and IV) during the re-heating phase. In (c), the relative difference of T_e before ($t = 15.6710$ s) and after ($t = 15.6727$ s) the crash is displayed. The radial positions where the difference is zero are defined as inversion radii.

the crash frequency is defined as the temporal interval between two consecutive crashes of the same type. Crashes are detected applying to ECE data a ridge detection algorithm, based on continuous wavelet transform (CWT) [32]. Since crashes of different amplitude are detected, we sort them into two types, according to their amplitude. Type A events are those overcoming a certain amplitude threshold, while type B are those events with amplitude below the choosen threshold and occurring between two type A events. The crash parameters, i.e. inversion radii, the temporal intervals and the amplitudes of both crash types exhibit a strong time dependent behaviour analysed in the following.

4.1. Crash classification: Type A-crash

Figure 8 shows the evolution of the crash parameters for the two crash types. The inversion radius (first plot of figure 8) and the amplitude (third plot) increase in time, with crashes in the latter stage of the discharge reaching an amplitude up to 60 % and causing a temporary decrease of the diamagnetic energy. The temporal interval (second plot of figure 8) between type A crashes increases from 0.05 s to 0.5 s and saturates after 8 s. Temperature oscillations caused by sawtooth precursors are detected in most crashes at the beginning of the discharge. The oscillating precursor phase becomes shorter as the discharge evolves, until the oscillating precursors become not recognisable anymore from the noise and only the core displacement is observed before the temperature crash. The amplitude and the expulsion region increase with current (see figures 2(a) and (b)). One can assume that this is related to an outward shift of the position where the resonance is reached. Since T_e , n_e and the beam deposition region do not change during the experimental program, the increase of r_{inv} has to be primarly caused by a change in the position of $r_{\iota=1}$, caused

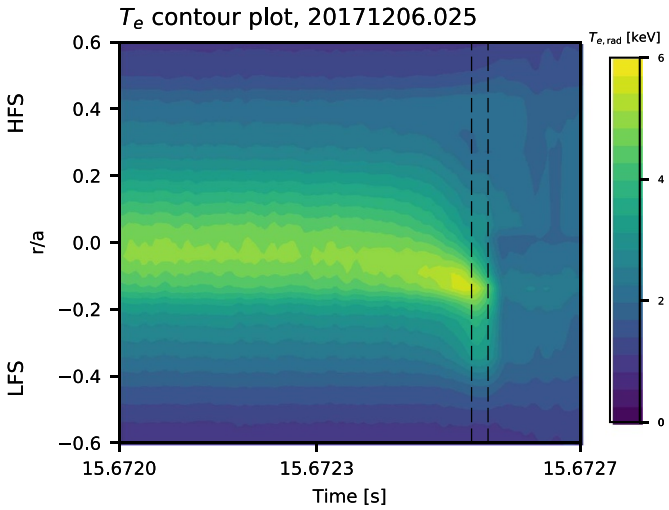

Figure 6. Contour plot of a crash, using ECE data. No precursors are visible before the crash. The core dispacement, from centre to low field side, is visible at 15.672 5 s, before the crash. The crash phase is highlighted by the two dashed lines and occurs within 25 μs. The temperature flattening observed at the same time at $r/a \approx 0.3$ may represent the development of a magnetic island.

in turn by an increase of the toroidal current enclosed in this plasma volume. This increase can be explained by assuming that the current density is more intense in the proximity of the deposition region, which is inside the inversion radius, and, therefore, most of the current be inside this region, thus shifting $r_{\iota=1}$ outwards. Presently this hypothesis can not be confirmed with experimental data, since direct measurements of the current density are not yet available at W7-X, however this hypothesis can be supported by the relation between the measured toroidal current and the crash amplitude evolution (compare figures 2(*b*) and (*d*)). The instantaneous onset of sawtooth oscillations suggests that, in principle, even small values of peaked and localised toroidal current can cause it, through a mild distortion of the vacuum rotational transform profile.

4.2. Crash classification: Type B-crash

The presence of the smaller crashes, which occur between the type A events, can be detected after some seconds, as the temporal interval between main crashes has increased. In these intermediate events the main features of the big crashes are reproduced: fast crash of the temperature in the core and a moderate increase in the external part. The crash amplitude varies between 10 % and 35 %, while the temporal interval between these crashes is about 0.01 s. The mode analysis carried out in section 3 is now more difficult: these events are hardly detected by the soft x-ray tomography diagnostic and being well localised in a narrower radial region than the type A crashes, as seen in figure 8. Consequently it was not possible to detect a relevant displacement of the core before the crash itself. If we consider the time window where the current and the crash amplitude have saturated, we notice that the pattern of type B-crashes is very regular: after every type A crash, small crashes with small amplitudes are detected. Between two type A crashes the amplitude and the temporal interval between type B crashes increase and saturates, untill the netx type A crash occurs (figure 3).

The presence of smaller crashes occuring in a narrower region close to the magnetic axis may be caused by a crossing of $\iota = 1$ close to the magnetic axis. This hypothesis can not be confirmed, but it is not contraddicted by the calculations discussed in section 5.1.

5. Heuristic iota evolution model

At W7-X the so-called standard configuration (standard magnetic field configuration) has a $\iota_{\rho=0} = 0.85$ and $\iota_{\rho=a} = 0.97$, so major resonances are avoided. Nevertheless, if a toroidal current is present, it can be written as a combination of two terms:

$$\iota = \iota_{vac} + \iota_{\mathrm{curr}} \tag{2}$$

where ι_{vac} is the rotational transform created by magnetic coils only and ι_{curr} is the contribution to the rotational transform given by toroidal currents. $\iota(r)_{\mathrm{curr}} \propto I(r)/r^2$, with $I(r)$ the toroidal current enclosed in the plasma volume of radius r. The $1/r^2$ dependence, together with W7-X being a low shear stellarator, makes the rotational transform very sensitive to local changes of toroidal current, such as ECCD. Examples of modified ι profiles are plotted in figure 9.

In section 5.1 we introduce a 1-D cylindrical model in order to estimate the typical timescale for the onset of the sawtooth instability. A 1-D cylindrical model is insufficient to describe the complexity of the stellarator geometry but can be used to provide a first quantitative guess of the current drive effects on the rotational transform profile. This approach is justified by the fact that the ECCD is driven in the proximity of the axis, inside $r_{\mathrm{eff}}/a < 0.25$. This fact, along with being W7-X a large aspect stellarator ($R/a \approx 10$) allows for using a 1-D cylindrical approximation as a first step to evaluate the current profile evolution. In 5.2 we estimate the role of the toroidal current in determining the position where the instability can be triggered.

5.1. 1-D current diffusion model

The current density $j_{\mathrm{tot}}(r,t)$ is composed of three terms: $j_{\mathrm{BS}}(r)$, $j_{\mathrm{ECCD}}(r)$ and $j_{\mathrm{ind}}(r,t)$: $j_{\mathrm{BS}}(r)$ is the bootstrap current (calculated by the NTSS code [33]), $j_{\mathrm{ECCD}}(r)$ is the ECCD (calculated by the ray-tracing code TRAVIS.) and $j_{\mathrm{ind}}(r,t)$ is the shielding current. The plasma, due to Lenz's law, generates the latter to oppose magnetic flux changes. For the TRAVIS calculation of $j_{\mathrm{ECCD}}(r)$ the magnetic equilibrium reconstruction has been calculated with VMEC. No additional recalculations of the magnetic equilibrium due to toroidal current changes have been performed. $j_{\mathrm{ECCD}}(r)$ and $j_{\mathrm{ind}}(r,t)$ are plotted in figure 10a (dashed lines). ECCD is strongly peaked and generated inside

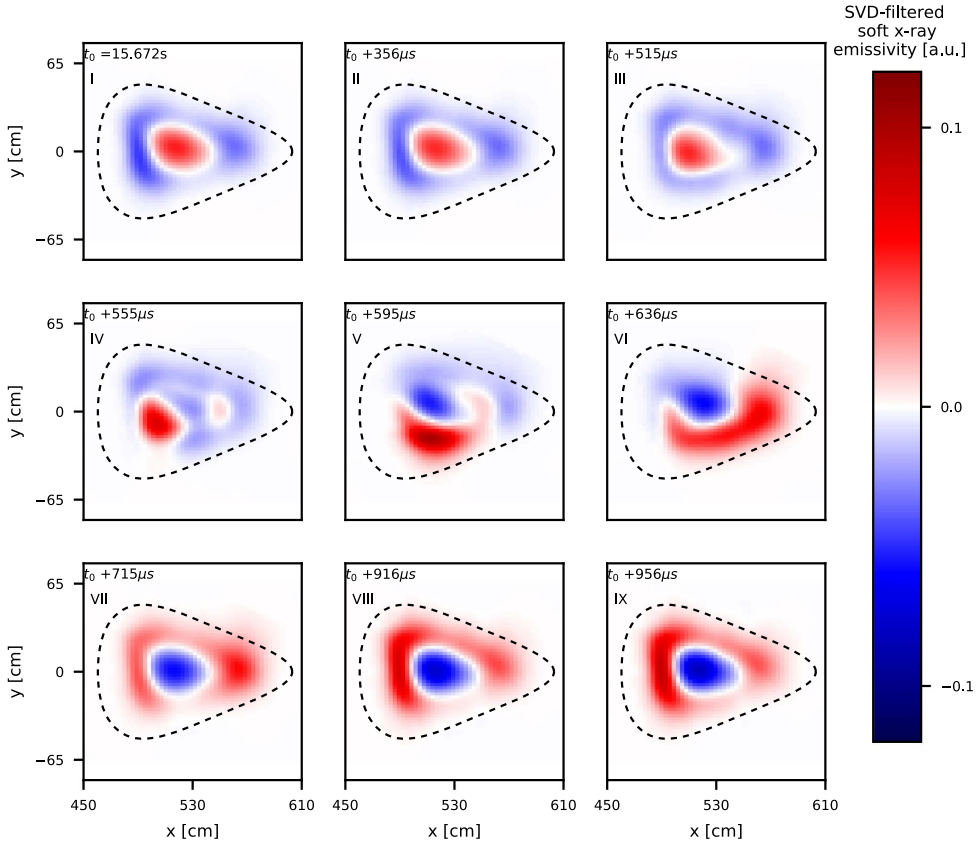

Figure 7. SVD-filtered soft x-ray tomographic reconstruction of a sawtooth crash at W7-X. The black dashed curve represents an estimation of the LCFS. Tomographic data have been SVD-filtered by removing the dominant component, which for this case consisted of a constant value. Plot (I) shows the plasma at the equilibrum. In II and III the development of the displacement (from core to high field side) is depicted. In IV the core is expelled and rotates (V, VI, VII) in anti-clockwise direction. In VIII and IX the poloidal symmetry is restored.

$r/a < 0.25$, while the boostrap current has a very broad profile. If $j_{\mathrm{ECCD}}(r)$ is constant in time, $j_{\mathrm{ind}}(r,t)$ evolves as:

$$\mu_0 \frac{\partial j_{\mathrm{ind}}(r,t)}{\partial t} = \frac{1}{r}\frac{\partial}{\partial r}\left(r\frac{\partial}{\partial r}(\eta_{\mathrm{sp}}(r) j_{\mathrm{ind}}(r,t))\right) \tag{3}$$

with μ_0 being the vacuum permeability, $\eta_{\mathrm{sp}}(r)$ the Spitzer plasma resistivity ([30]) and $j_{\mathrm{ind}}(r,0) = -(j_{\mathrm{ECCD}}(r) + j_{\mathrm{BS}}(r))$. In figure 10 the numerical solution of equation (3) is plotted for three different timesteps (solid lines). The shielding current diffuses mainly towards the centre, allowing for a strong and localised current density increase on a timescale faster than the skin time. In the right plot of figure 10 the sum of currents is displayed for different timesteps.

In 1-D cylindrical geometry, the rotational transform produced by the toroidal current can be written as:

$$\iota_{\mathrm{curr}}(r) = \frac{\mu_0 R_0 I_{\mathrm{tor}}(r)}{2\pi B_{\mathrm{tor}} r^2}. \tag{4}$$

Therefore, because the toroidal current and the rotational transform are connected, it is possible to express equation (3) as:

$$\frac{\partial \iota_{\mathrm{ind}}}{\partial t} = \frac{1}{\mu_0 r}\frac{\partial}{\partial r}\left[\frac{\eta_{\mathrm{sp}}}{r}\frac{\partial}{\partial r}\left(r^2 \iota_{\mathrm{ind}}\right)\right]. \tag{5}$$

Equation (5) describes the resistive evolution of the rotational transform. Taking this into account, considering neoclassical corrections, as discussed in [34], and renormalising equation (3) with respect to the resistive time $\tau_\eta = \mu_0 l^2/\eta_0$, where η_0 is the Spitzer resistivity in the core and l is a characteristic length:

$$\frac{\partial \iota_{\mathrm{ind}}}{\partial \tau} = \frac{1}{\hat{r}}\frac{\partial}{\partial \hat{r}}\left[\frac{\hat{\eta}}{\hat{r}}\frac{\partial}{\partial \hat{r}}\left(\hat{r}^2 \iota_{\mathrm{ind}}\right)\right] \tag{6}$$

with $\tau = t/\tau_\eta$, $\hat{r} = r/l$, and $\hat{\eta} = \eta_{sp}/\eta_0$. The rotational transform of the system is finally given by equation (2), with $\iota_{\mathrm{curr}}(r,t) = \iota_{\mathrm{ind}}(r) + \iota_{\mathrm{ECCD}}(r) + \iota_{\mathrm{BS}}(r)$, the latters being respectively the rotational transform modifications due to stationary ECCD and stationary bootstrap current, i.e. the modifications of ι after several L/R times. At $t = 0$, the initial condition is $\iota_{\mathrm{ind}}(r, t = 0) = -(\iota_{\mathrm{ECCD}}(r) + \iota_{\mathrm{BS}}(r))$.

If the crash is triggered by the resistive diffusion of ι, the diffusion has to occur on a timescale of $\Delta\tau_\eta \approx \Delta t_{\mathrm{crash}} \approx 0.2$ s on a characteristic spatial scale l, that in this case represents the skin depth. For the plasma parameters of the discussed discharge in this paper, $\Delta\tau_\eta$ can be expressed as $\Delta\tau_\eta \approx 500\, l^2\, \mathrm{s/m^2}$, therefore $l \approx 2$ cm. The numerical solution of equation (6) at different times is plotted in figure 11.

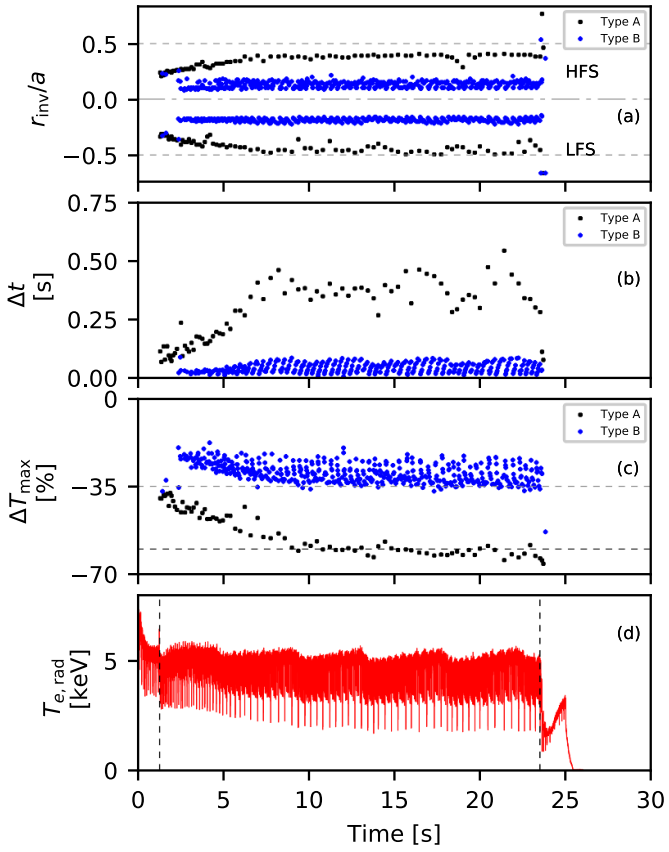

Figure 8. Temporal evolution of the inversion radii (r_{inv}), crash interval (Δt) and crash amplitude (ΔT_{max}) as a function of time from $t = 1.3$ s to $t = 23.5$ s (dashed lines in the bottom plot). In the first plot the r_{inv} of both crash types is displayed. It is possible to notice a relevant outward shift for type A crash. In the second plot, the temporal interval between two crashes of the same type is plotted. Δt for type A crashes strongly increases in the first 10 s of the discharge, from 100 ms to around 400 ms. In the third plot, ΔT_{max} is plotted. For type A crashes the amplitude goes from $-35\,\%$ to $-70\,\%$. For type B crashes, the amplitude increases and saturates until the next type A crash. (Also see figure 3).

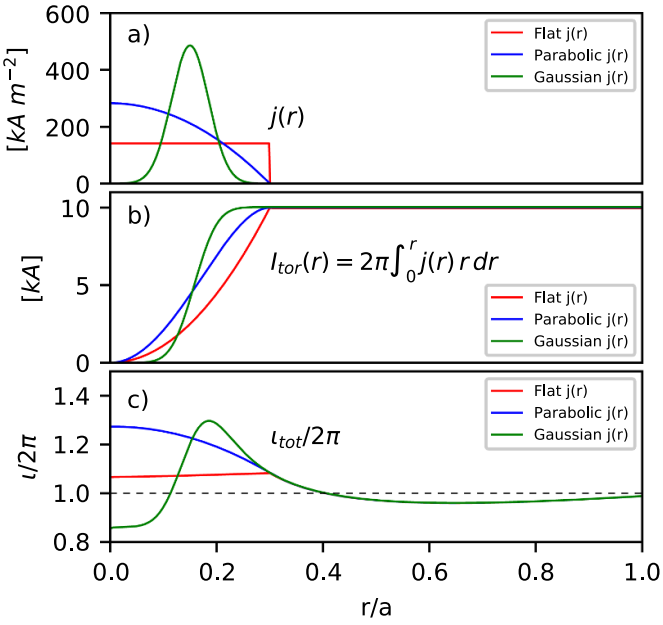

Figure 9. Sketch of rotational transform modification due to a toroidal current. In (*a*) , three different current density profiles are plotted: a flat current profile (red) , a parabolic profile (blue) and a Guassian profile (green). The three profiles yield the same toroidal current when integrated on the whole plasma volume. In (*b*) the toroidal current is plotted as a function of the radius. In (*c*) the modified ι profiles are plotted. The dashed line indicates the resonance $\iota = 1$.

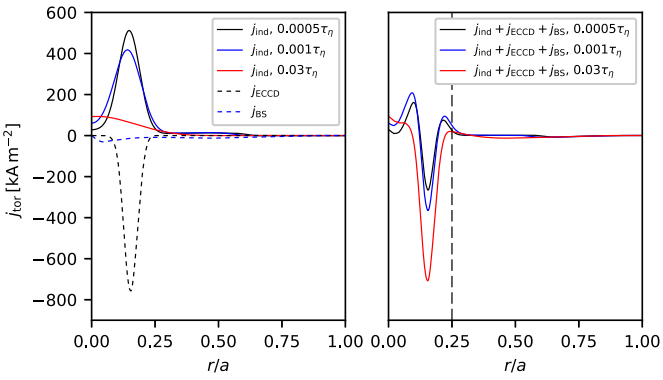

Figure 10. Modelled current density profiles for different timesteps. On the left image, $j_{ECCD}(r)$, $j_{BS}(r)$ (dotted lines) and $j_{ind}(r,t)$ are plotted. $j_{ind}(r,t)$ represents the numerical solution of equation (3), without taking into account any current redistribution after a crash. The shielding current $j_{ind}(r,t)$ diffuses towards the centre and a net current is created. On the right image the sum of the two components is displayed. The dashed vertical line represents the position of r_{inv} at the beginning of the discharge.

The ECCD modifies the rotational transform and a low order rational value is reached on the order of $0.0012\tau_\eta \approx 74$ ms, which is consistent with the measured time for sawtooth activity to start. The red curve represents the case where almost the whole shielding current is dissipated and no current redistribution has been taken into account. Ideally a double crossing of $\iota = 1$ is possible. The dominant contribution is given by ECCD, being it deposited close to the axis with a stronly peaked profile. For the calculated current profiles, the contribution of the bootstrap current inside r_{inv} i.e. for $r/a < 0.4$ is less than $10\,\%$.

The presented model presents two main limits. Since the sawtooth crash can introduce significant changes on the current profile and since no current redistribution has been introduced yet, we presently use this model to estimate the ι profile at the beginning of the discharge only. The strong dependence of $\iota_{curr}(r) \propto I(r)/r^2$ makes our model no longer valid in the axis, where the rotational transform is strongly affected. In the axis a strong current can change also the toroidal flux

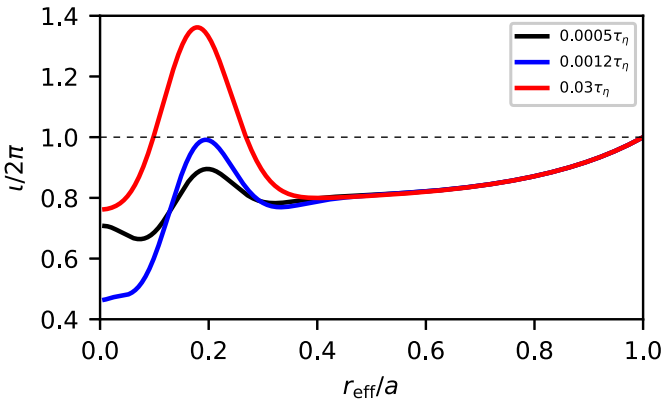

Figure 11. Modelled rotational transform profile modified by ECCD for different times. Plotted curves represent the solution of equation (5).

[35] and therefore the crossing of $\iota = 0.5$ is not taken into consideration.

5.2. Estimation of r_{inv}

Here we present an estimation of $r_{\iota=1}$ for type-A crashes based on two major observations. The first assumption is that the driven toroidal current is mainly generated in the proximity of the magnetic axis, therefore it is deposited inside the measured r_{inv}. The second observation concerns the bootstrap current, which has been calculated to be about 3 kA in the stationary phase, with a broad profile. Combining these assumptions, we can assume the toroidal current density to be mainly distributed inside r_{inv} and therefore that the measured toroidal current yields a good estimation of the toroidal current inside the inversion radius, i.e. $I_{\mathrm{tor}}(r = a) \approx I_{\mathrm{tor}}(r_{\iota=1})$, where $I_{\mathrm{tor}}(r_{\iota=1}) = 2\pi \int_0^{r_{\iota=1}} j_{\mathrm{tor}}(r)\, r\, \mathrm{d}r$, with $r_{\iota=1}$ being the radius where $\iota = 1$ is crossed. The assumption that the majority of the current is distributed close to the magnetic axis allows us to estimate $\iota = 1$ despite the lack of information about the real $j(r)$ profile. As plotted in figure 10, the crossing position depends only on the integrated value of $j(r)$, which corresponds with this assumption to the experimentally measured toroidal current.

We used equation (2) and equation (4) to estimate how the rotational transform is modified by the toroidal current. For every detected crash, we calculated $r_{\iota=1}$, which is the radial position that solves equation (2) and compared it to the inversion radius (r_{inv}) of every crash as displayed in figure 12. The temporal evolution of the calculated $r_{\iota=1}$ position follows the trend of r_{inv} increase. While at the beginning of the discharge the two positions deviate approximately by 25% , the deviation is reduced in time, until the two datasets differ by less than 10 %. This deviation indicates that r_{inv} and $r_{\iota=1}$ might not coincide. The initial bigger difference can have different explanation. At the beginning of the dischage, due to the shielding current $j_{\mathrm{ind}}(r,t)$, the toroidal current inside the inversion radius does not represents the whole toroidal current measured by the

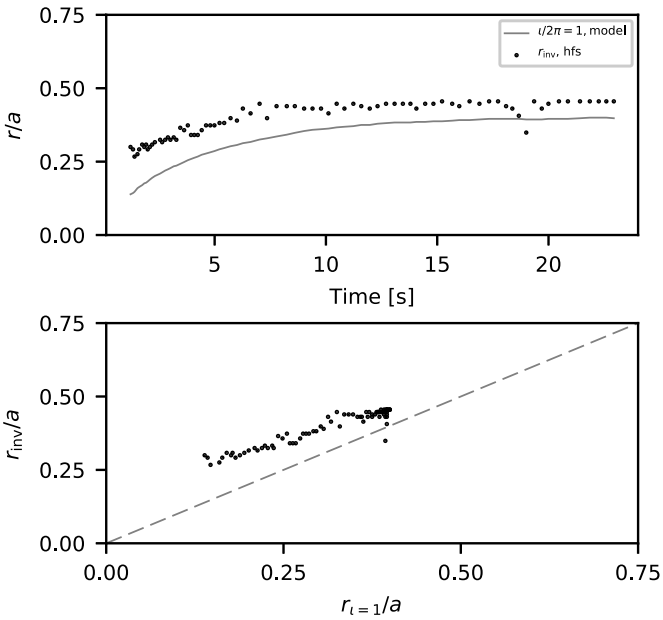

Figure 12. Comparison between the inversion radii r_{inv} obtained by experimental data and $r_{\iota=1}$, which represents the radial position that satisfies $\iota = 1$. In the top plot, the two quantities are plotted as a function of time. In the bottom plot r_{inv} is plotted against $r_{\iota=1}$. The dashed grey line represents the line $x = y$.

Rogowski coils. Other issues are geometrical factors neglected in the cylindrical approximation, which could have an higher impact close to the axis. Although r_{inv} and $(r_\iota = 1$ do not coincide, it is interesting to notice that they follow a similar trend (bottom plot of figure 12) and their difference becomes constant at the end of the discharge. This confirms that the increase of the crash size is caused by the toroidal current increase inside r_{inv}.

6. Discussion and conclusions

In this work we presented a typical ECCD experiment with sawtooth-like activity at the W7-X stellarator.

W7-X is a low shear stellarator which relies on the existence of magnetic island chains at the plasma edge. The strikeline control on the divertor plates is necessary in order to avoid component damages. However it was found that a localised current, such as ECCD can induce local changes to the rotational transform, thus making the plasma susceptible to MHD instability. The presence of strong ECCD seems to be fundamental for the trigger of the sawtooth crashes at W7-X. No sawtooth crashes have been observed so far in experiments without ECCD.

In typical ECCD programs, two crash types can be distinguished, whose parameters (such as crash amplitude, inversion radius and temporal interval between them) change in time. For stronger temperature crashes a mode structure, consistent with a (1, 1) mode, is detected before the crash. In many cases, the precursor is a pure displacement and no temperature

oscillations are detected. Precursors are generally associated to diamagnetic rotation: at the beginning of the discharge, these crashes occur in a region with higher ∇p (and therefore, stronger diamagnetic rotation). As the crash localisation moves outwards, ∇p decreased the and rotation is strongly reduced.

Considering the operational regimes and the characteristic times for the instability to grow, a potential explanation for the mechanism could be: 1) current drive drastically changes the iota profile, eventually crossing resonant values. 2) An internal (1, 1) non ideal kink is destabilised, as discussed in [20–22]. 3) The fast movement of the core and the deformation of the pressure profile creates a narrow region were ∇p is increased. 4) The point of the plasma between the displaced core and the unperturbed external magnetic surfaces represents the X-point were magnetic reconnection takes place, allowing for a fast redistribution of pressure. In the analysed experiments the core is expelled outside the $\iota = 1$ region in about 20 μs, consistent with the results of [21], and rotates in the direction of the electron diamagnetic drift. Two different types of crashes have been observed, with different amplitudes and temporal intervals. This analysis has been conducted for bigger crashes: smaller crashes are more difficult to resolve. The coupling between these two types of crash is still unclear, but an initial explanation assumes a double resonance crossing, on different positions. The two modes, nevertheless, seem to develop on distinct timescales. A 1-D model has been developed, to estimate typical timescales for the ι evolution. We found that the modifications caused by the current drive is fast and strong enough to produce resonant values consistent with experimental results. The main contribution to the rotational transform modifications is given by ECCD, which is stronly peaked and localised close to the axis. The bootstrap current, having a very broad profile, yields a negligible contribution to the net toroidal current in the region where crashes are detected. This model is valid only for the initial events, since no current redistribution caused by the instabilities has been implemented yet. Nonetheless, combining equation (2) and equation (4), we have been able to find a relation between r_{inv} and I_{tor}, which explain the crash size increase. As the current develops, the $r_\iota = 1$ position moves outwards, thus leading to a bigger crash amplitude. Further investigations, using MHD codes, are still ongoing, in order to confirm experimental observations about the nature and characteristic times of mode developement.

Acknowledgments

We thank Valentin Igochine and Joachim Geiger for several insightful discussions. This work has been carried out within the framework of the EUROfusion Consortium and has received funding from the Euratom research and training programme 2014-2018 and 2019-2020 under Grant Agreement No. 633053. The views and opinions expressed herein do not necessarily reflect those of the European Commission.

ORCID iDs

M. Zanini https://orcid.org/0000-0002-8717-1106
C. Brandt https://orcid.org/0000-0002-5455-4629
K.J. Brunner https://orcid.org/0000-0002-0974-0457
J. Schilling https://orcid.org/0000-0002-6363-6554
R.C. Wolf https://orcid.org/0000-0002-2606-5289
A. Zocco https://orcid.org/0000-0003-2617-3658

References

[1] Wolf R. *et al* 2017 *Nucl. Fusion* **57** 102020
[2] Wolf R. *et al* 2019 *Phys. Plasmas* **26** 082504
[3] Stang T. *et al* 2017 *EPJ Web Conf.* **157** 02008
[4] Fisch N.J. and Boozer A.H. 1980 *Phys. Rev. Lett.* **45** 720–2
[5] Erckmann V. and Gasparino U. 1994 *Plasma Phys. Control. Fusion* **36** 1869–1962
[6] Geiger J. *et al* 2010 *Contrib. Plasma Phys.* **50** 770–4
[7] Geiger J. *et al* 2011 *Contrib. Plasma Phys.* **51** 99–99
[8] Sunn Pedersen T. *et al* 2019 *Plasma Phys. Control. Fusion* **61** 014035
[9] Gao Y. *et al* 2019 *Nucl. Fusion* **59** 106015
[10] Wolf R. *et al* 2019 *Plasma Phys. Control. Fusion* **61** 014037
[11] von Goeler S., Stodiek W. and Sauthoff N. 1974 *Phys. Rev. Lett.* **33** 1201–3
[12] Weller A. *et al* 2001 *Phys. Plasmas* **8** 931–56
[13] Estrada T. *et al* 2002 *Plasma Phys. Control. Fusion* **44** 1615–24
[14] Nagayama Y. *et al* 2003 *Phys. Rev. Lett.* **90** 205001
[15] Nicolas T. *et al* 2014 *Phys. Plasmas* **21** 012507
[16] Yamada I., Yamazaki K., Oishi T., Arimoto H. and Shoji T. 2008 Transport analysis of high-Z impurity with MHD effects in tokamak system *Proc. ITC18* (Gifi, Japan, 9–12 December 2008) P1.27 (https://www.nifs.ac.jp/itc/itc18/upload/proceedings_upload/proc_P1-27_Yamada.pdf)
[17] Wesson J. and Campbell D.J. 2004 *Tokamaks* (Oxford: Oxford University Press) p 365
[18] Kadomtsev B.B. 1975 *Fiz. Plasmy* **1** 710–15
[19] Chapman I.T. 2010 *Plasma Phys. Control. Fusion* **53** 013001
[20] Strumberger E. and Günter S. 2020 *Nucl. Fusion* **60**
[21] Yu Q. *et al* 2020 *Nucl. Fusion* **60** 076024
[22] Zocco A., Mishchenko A. and Könies A. 2019 *J. Plasma Phys.* **85** 905850607
[23] Hirsch M. *et al* 2019 *EPJ Web of Conferences* **203** 03007
[24] Höfel U. *et al* 2019 *Rev. Sci. Instrum.* **90** 043502
[25] Brandt C. *et al* 2020 *Plasma Phys. Control. Fusion* **62** 035010
[26] Brunner K.J. *et al* 2018 *JINST* **13** P09002–P09002
[27] Rahbarnia K. *et al* 2018 *Nucl. Fusion* **58** 096010
[28] Marushchenko N.B., Turkin Y. and Maassberg H. 2014 *Comput. Phys. Commun.* **185** 165–76
[29] Hirshman S.P. and Whitson J.C. 1983 *Phys. Fluids* **26** 3553
[30] NRL *Plasma Formulary* (U.S.: Naval Research Laboratory)
[31] Dudok de Wit T. *et al* 1994 *Phys. Plasmas* **10** 3288–300
[32] Mallat S. 2009 *A Wavelet Tour of Signal Processing* (Amsterdam: Elsevier)
[33] Turkin Y. *et al* 2011 *Phys. Plasmas* **18** 022505
[34] Zocco A. *et al* 2013 *Plasma Phys. Control. Fusion* **55** 074005
[35] Strand P.I. and Houlberg W.A. 2001 *Phys. Plasmas* **8** 2782–92